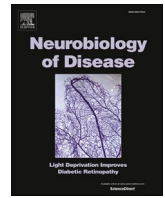


## **Disturbed brain energy metabolism in a rodent model of DYT-TOR1A dystonia**

**Susanne Knorr, Lisa Rauschenberger, Muthuraman Muthuraman, Rhonda McFleder, Thomas Ott, Kathrin Grundmann-Hauser, Takahiro Higuchi, Jens Volkmann, Chi Wang Ip**

### **Angaben zur Veröffentlichung / Publication details:**

Knorr, Susanne, Lisa Rauschenberger, Muthuraman Muthuraman, Rhonda McFleder, Thomas Ott, Kathrin Grundmann-Hauser, Takahiro Higuchi, Jens Volkmann, and Chi Wang Ip. 2024. "Disturbed brain energy metabolism in a rodent model of DYT-TOR1A dystonia." *Neurobiology of Disease* 194: 106462. <https://doi.org/10.1016/j.nbd.2024.106462>.



## Disturbed brain energy metabolism in a rodent model of DYT-TOR1A dystonia

Susanne Knorr<sup>a</sup>, Lisa Rauschenberger<sup>a</sup>, Muthuraman Muthuraman<sup>a</sup>, Rhonda McFleder<sup>a</sup>, Thomas Ott<sup>b,c,d</sup>, Kathrin Grundmann-Hauser<sup>b,e</sup>, Takahiro Higuchi<sup>f</sup>, Jens Volkmann<sup>a</sup>, Chi Wang Ip<sup>a,\*</sup>

<sup>a</sup> Department of Neurology, University Hospital Würzburg, 97080, Germany

<sup>b</sup> Institute for Medical Genetics and Applied Genomics, University of Tübingen, 72076, Germany

<sup>c</sup> Core Facility Transgenic Animals, University Hospital of Tübingen, 72076, Germany

<sup>d</sup> Max Planck Institute for Biological Cybernetics, Tübingen, 72076, Germany

<sup>e</sup> Centre for Rare Diseases, University of Tübingen, 72076, Germany

<sup>f</sup> Department of Nuclear Medicine, University Hospital Würzburg, 97080, Germany

### ARTICLE INFO

#### Keywords:

Dystonia  
DYT-TOR1A  
Sciatic nerve crush injury  
Brain energy metabolism  
Fatty acid  $\beta$ -oxidation  
Glucose  
Fenofibrate

### ABSTRACT

DYT-TOR1A (DYT1) dystonia, characterized by reduced penetrance and suspected environmental triggers, is explored using a “second hit” DYT-TOR1A rat model. We aim to investigate the biological mechanisms driving the conversion into a dystonic phenotype, focusing on the striatum’s role in dystonia pathophysiology.

Sciatic nerve crush injury was induced in  $\Delta$ ETorA rats, lacking spontaneous motor abnormalities, and wild-type (wt) rats. Twelve weeks post-injury, unbiased RNA-sequencing was performed on the striatum to identify differentially expressed genes (DEGs) and pathways. Fenofibrate, a PPAR $\alpha$  agonist, was introduced to assess its effects on gene expression. <sup>18</sup>F-FDG autoradiography explored metabolic alterations in brain networks.

Low transcriptomic variability existed between naïve wt and  $\Delta$ ETorA rats (17 DEGs). Sciatic nerve injury significantly impacted  $\Delta$ ETorA rats (1009 DEGs) compared to wt rats (216 DEGs). Pathway analyses revealed disruptions in energy metabolism, specifically in fatty acid  $\beta$ -oxidation and glucose metabolism. Fenofibrate induced gene expression changes in wt rats but failed in  $\Delta$ ETorA rats. Fenofibrate increased dystonia-like movements in wt rats but reduced them in  $\Delta$ ETorA rats. <sup>18</sup>F-FDG autoradiography indicated modified glucose metabolism in motor and somatosensory cortices and striatum in both  $\Delta$ ETorA and wt rats post-injury.

Our findings highlight perturbed energy metabolism pathways in DYT-TOR1A dystonia, emphasizing compromised PPAR $\alpha$  agonist efficacy in the striatum. Furthermore, we identify impaired glucose metabolism in the brain network, suggesting a potential shift in energy substrate utilization in dystonic DYT-TOR1A rats. These results contribute to understanding the pathophysiology and potential therapeutic targets for DYT-TOR1A dystonia.

### 1. Introduction

Dystonia is a movement disorder with a heterogeneous clinical picture characterized by involuntary muscle contractions leading to abnormal movements or postures (Albanese et al., 2013). The most common monogenetic form of dystonia is early-onset isolated dystonia (DYT-TOR1A; DYT1) with disease onset in childhood or early adolescence. Most cases of DYT-TOR1A dystonia are linked to a heterozygous three-base pair ( $\Delta$ GAG;  $\Delta$ E) deletion in the coding region of the *TOR1A*

gene, which results in loss of a glutamic acid residue at position 302 or 303 of the corresponding ATP-binding protein torsinA (Ozelius et al., 1997). TorsinA belongs to the AAA+ (ATPases associated with various cellular activities) protein family and it is ubiquitously expressed in all tissues (Hanson and Whiteheart, 2005; Ozelius et al., 1997; Shashidharan et al., 2000). In the brain, high torsinA mRNA expression patterns are present in dopaminergic neurons of the substantia nigra (SN) pars compacta. In addition, in the striatum, cerebral cortex, hippocampus, SN, globus pallidus (GP), brainstem, thalamus, cerebellum,

\* Corresponding author at: Department of Neurology, University Hospital of Würzburg, Josef-Schneider-Straße 11, 97080 Würzburg, Germany.

E-mail address: [ip\\_c@ukw.de](mailto:ip_c@ukw.de) (C.W. Ip).

<https://doi.org/10.1016/j.nbd.2024.106462>

Received 17 January 2024; Received in revised form 21 February 2024; Accepted 1 March 2024

Available online 3 March 2024

0969-9961/© 2024 The Authors. Published by Elsevier Inc. This is an open access article under the CC BY-NC license (<http://creativecommons.org/licenses/by-nc/4.0/>).

and spinal cord different mRNA and protein expression levels of torsinA were detected (Augood et al., 2003; Augood et al., 1999; Augood et al., 1998; Shashidharan et al., 2000). The localization of torsinA is described for the endoplasmic reticulum (ER) and the nuclear envelope (NE) (Hewett et al., 2000; Hewett et al., 2003; Kustedjo et al., 2000; Naismith et al., 2004). It has been linked to various functions, including intracellular trafficking (Kamm et al., 2004), synaptic vesicle exocytosis (Granata et al., 2008), ER-associated degradation (Nery et al., 2011), and the regulation of the lipid metabolism (Grillet et al., 2016). However, despite these associations, the functional spectrum of both torsinA and its mutated form (torsinA( $\Delta E$ )) remains incompletely characterized. While the precise mechanisms by which the mutated torsinA (torsinA( $\Delta E$ )) gives rise to DYT-TOR1A dystonia remain poorly understood, it is hypothesized that the genetic mutation within the *TOR1A* gene and the subsequent synthesis of the torsinA( $\Delta E$ ) protein establish the fundamental basis of DYT-TOR1A dystonia.

Because of the observed reduced disease penetrance of approximately 30–40%, disease modifiers are deemed essential for the manifestation of DYT-TOR1A dystonia. Environmental factors such as physical trauma or stressful events are assumed to act as potential triggers in individuals with DYT-TOR1A dystonia (Edwards et al., 2003; Gioltzoglou et al., 2006; Martino et al., 2013). In accordance with this observation, dystonia-like movements (DLM) were successfully induced by unilateral peripheral nerve injury in several genetic DYT-TOR1A rodent models (Ip et al., 2016; Knorr et al., 2021; Rauschenberger et al., 2023), including the transgenic DYT-TOR1A rat ( $\Delta E$ TorA) that carries the full-length human mutant *TOR1A* gene ( $\Delta E$ ) (Grundmann et al., 2012). Long-lasting focal DLM in the injured hindlimb was evident in nerve-injured  $\Delta E$ TorA rats. This model further demonstrated significantly increased theta power in the entopeduncular nucleus (EP), serving as the rat counterpart of the human globus pallidus internus (GPI), as well as within the motor cortex. Notably, this elevated theta power could be modulated by deep brain stimulation (DBS) of the EP, resulting in concurrent alleviation of DLM. Furthermore, an increased striatal dopamine metabolism was also noted in nerve-injured  $\Delta E$ TorA rats (Knorr et al., 2021). The similarity to human DYT-TOR1A dystonia in terms of pathophysiology demonstrates the translational value of the  $\Delta E$ TorA rat model. Moreover, another advantage of this model lies in its capacity to distinguish between the endophenotype resulting from the expression of the human *TOR1A* mutation and the network changes associated with the onset of DLM following sciatic nerve crush injury. Another crucial aspect of the  $\Delta E$ TorA rat model is the overexpression of the human mutant torsinA protein. However, it remains unclear whether the mutation of the *TOR1A* gene itself leads to a gain of function, a loss of function, or both, and whether the overexpression of the *TOR1A* gene also contributes to this. Furthermore, the expression pattern of the torsinA protein observed in the human brain is not faithfully replicated in the rodent model. Neuropathologically, severely altered ultrastructural changes in the nuclear envelope have been detected in various brain regions of  $\Delta E$ TorA rats, a phenomenon not described in the human brain. Consequently, the potential impact of high expression levels on this phenotype in the  $\Delta E$ TorA rats cannot be ruled out (Grundmann et al., 2012).

By utilizing the  $\Delta E$ TorA rat model, we conducted RNA-sequencing (RNA-seq) of striatal tissue. This approach revealed a multitude of differentially expressed genes (DEGs) and identified novel potential pathways contributing to the underlying pathophysiology of dystonia. Given that our data suggested a potential involvement of energy metabolism in dystonia, we administered fenofibrate to nerve-injured wt and  $\Delta E$ TorA rats to evaluate its impact on the expression of genes associated with energy metabolism. Fenofibrate, a fibric acid derivative, has been in clinical use for decades, acting through the activation of peroxisome proliferator-activated receptor-alpha (PPAR $\alpha$ ). PPAR $\alpha$  serves as a master regulator, governing the expression of genes involved in diverse metabolic processes, encompassing lipid metabolism, glucose homeostasis, inflammation, and energy metabolism (Rakhshandehroo et al., 2010). In

specific contexts, PPAR $\alpha$  can influence the activity of hundreds to thousands of genes. For instance, in the liver, PPAR $\alpha$  regulates the expression of numerous genes involved in fatty acid oxidation and ketogenesis (Rakhshandehroo et al., 2009). Our findings indicate a critical involvement of energy metabolism pathways in the pathophysiology of DYT-TOR1A dystonia.

## 2. Materials and methods

### 2.1. Animals

Animals were bred in the animal facility of Tübingen and housed under standard conditions (21 °C, 12-h light/dark cycle) with free access to food and water. 61 transgenic hemizygous male  $\Delta E$ TorA rats and 73 male wild-type (wt) littermates on Sprague–Dawley background were used for the studies at the age of ten to twelve weeks. Genotyping was performed as previously described (Grundmann et al., 2012). All animal experiments were approved by the local government and performed in accordance with all applicable international, national, and/or institutional guidelines for care and use of animals.

### 2.2. Sciatic nerve crush injury

A right-sided sciatic nerve crush injury for 30 s was induced in deeply isoflurane/carprofen-anesthetized rats as previously described (Ip et al., 2016; Knorr et al., 2021).

### 2.3. Drug treatment

Treatment with fenofibrate (PPAR $\alpha$  agonist, E8200 Version 0016, SAFE, Augy, France) was delivered to 16 wt and 14  $\Delta E$ TorA nerve-injured rats that were randomly selected three weeks after nerve crush injury and assigned to a non-treated group with a standard chow diet or a fenofibrate group with standard chow diet supplemented with fenofibrate (100 mg/kg body weight). The timing of treatment initiation was carefully chosen based on previously collected and published behavioral test data of this animal model (Knorr et al., 2021). These data indicate that three weeks after nerve crush injury, the animals have fully recovered from anesthesia and wound healing, with nerve function slowly improving and transition to DLM gradually beginning. After nine weeks of treatment with free access to drinking water, all rats were sacrificed (in total twelve week in experiment) for further analysis. 7 wt and 6  $\Delta E$ TorA nerve-injured rats were treated with a standard chow diet and 9 wt and 8  $\Delta E$ TorA nerve-injured rats were treated with standard chow diet supplemented with fenofibrate.

### 2.4. Tail suspension test (TST)

A TST was performed at the end of the experiment, twelve weeks after nerve crush injury in a blinded assessment. Rats were suspended by their tail and video recorded for 30 s. The videos were recorded at 50 frames per second and standardized for background and for the distance of the rat to camera.

### 2.5. Deep neural network and kinematic analyses

The software package DeepLabCut (Mathis et al., 2018) was used to track body features from the rats within the TST videos. The DeepLabCut network was trained on 184 frames extracted from TST videos not included in the final analysis. At a likelihood cutoff of 60% the deep neural network had a train error of 2.36 pix and a test error of 5.35 pix. 7 wt and 6  $\Delta E$ TorA nerve-injured rats treated with a standard chow diet, and 9 wt and 8  $\Delta E$ TorA nerve-injured rats treated with fenofibrate were included into behavioral analyses.

### 2.5.1. Functional and effective connectivity

Functional connectivity was assessed using the coherence measure, a tool utilized in the frequency domain to quantify the linear relationship between two signals recorded simultaneously. (Muthuraman et al., 2008). Kinematic marker time series from markers on the right hindlimb (RD2–4 (second to fourth digit tip), RHM (right hand mid), RC (right calcaneus), RKF (right knee front) and RKB (right knee back)) were compared with the left hindlimb markers, excluding those with likelihood <60%. The effective connectivity values were estimated using the temporal partial directed coherence method (TPDC) for the same kinematic markers mentioned above for both the right and left hindlimb. The TPDC method has been described previously (Muthuraman et al., 2018). The TPDC is a time-frequency causality technique, which is used to infer the strength of time-varying effective connectivity among time series (Ding et al., 2022). After estimating the TPDC values, the significance level was calculated from the applied data using a bootstrapping method (Kaminski et al., 2001). To create a new time series, we split the previous one into non-overlapping windows, shuffled them randomly, and fitted the shuffled time series with a multivariate autoregressive model to calculate TPDC. The shuffling was repeated 1000 times, and the average TPDC served as the significance threshold for all connections, done separately for each animal. The resulting value served as the significance threshold for all connections. We applied time reversal technique (Haufe et al., 2013) as a second significance test on the connections already identified by TPDC using data-driven bootstrapping surrogate significance testing.

### 2.5.2. Modularity

Modules were identified by applying the Louvain modularity algorithm (Blondel et al., 2008) in each individual rat connectivity matrix estimated based on coherence or TPDC. To test the robustness of the detected module association for the entire time interval, we performed 5000 iterations with the Louvain algorithm, where the assignment of each kinematic marker to a particular module was based on the maximum number of times/iterations a kinematic marker was assigned to a module (Ritchey et al., 2014).

### 2.6. Tissue preparation

Twelve weeks after nerve crush injury of the right sciatic nerve, rats were transcardially perfused with 0.1 M phosphate buffered saline. The striatum of the left hemisphere and the liver was dissected, stabilized in RNAlater solution (Qiagen, Hilden, Germany) for 24 h at 4 °C and snap-frozen in liquid nitrogen. mRNA of snap-frozen tissue was isolated by using RNeasy Micro Kit (Qiagen, Hilden, Germany) according to the guidelines of the manufacturer.

### 2.7. RNA-Sequencing (RNA-seq)

RNA concentration and purity were determined using the bio-analyzer 2100 (Agilent Technologies, Santa Clara, CA, USA). 80 ng of total RNA for each sample and 14 PCR cycles were used for library preparation according to the Illumina TruSeq stranded mRNA Sample Preparation Guide (Illumina, San Diego, CA, USA). Single-end sequencing with a read length of 75 nt in two runs of two times 14 libraries (28 samples) was performed on an Illumina NextSeq 500 system (Illumina, San Diego, CA, USA). After processing the reads using cutadapt (version 2.1), the reference genome was extended by NCBI RefSeq *Rattus norvegicus* Genome Rnor\_6.0 (<https://www.ncbi.nlm.nih.gov/genome/?term=txid101116>) and the sequence for the mutated human *TOR1A* gene (OMIM: 605204.0001) was added. Further, the reads were mapped to the processed sequences using STAR (STAR\_2.6.1a\_08–27) (Dobin et al., 2013). The number of reads were counted with the featureCounts from Subread package (version 1.6.3) (Liao et al., 2014). DEGs were identified using DESeq2 (version 1.22.2) (Love et al., 2014). *P*-values were corrected for multiple testing with the Benjamini-

Hochberg procedure. Genes with an adjusted *p*-value (padj) of <0.05 were considered as DEGs. Heatmaps were generated using R (version 3.6.2) and RStudio with the package “gplots”. Venn diagram was plotted with the web server “<http://bioinformatics.psb.ugent.be/webtools/Venn/>”. Functional enrichment analyses of pathways and gene ontologies were conducted using the web server “Enrichr” (Chen et al., 2013; Kuleshov et al., 2016). The reads per kilobase per million reads (RPKM) values were calculated according to Wagner et al., 2012 and used for the analyses of gene expression quantification (Wagner et al., 2012). Considering our specific research question aiming to identify pathways with differential expression regardless of the magnitude of change, and taking into account the limited number of DEGs present in the striatum, we adopted a cutoff criteria of padj <0.05 without considering log2FC values. This approach was chosen to screen for biological trends in the data when analyzing the number of up- and downregulated DEGs between pairwise comparisons of animal groups. 8 naïve wt, 8 naïve ΔETorA, 6 nerve-injured wt, and 6 nerve-injured ΔETorA rats were included into RNA-seq analysis.

### 2.8. Real-time PCR (qPCR)

cDNA was synthesized with SuperScrip IV VILO™ Master Mix (Thermo Fisher, Darmstadt, Germany) according to the guidelines of the manufacturer. qPCR was performed on triplicates for each sample together with commercially available TaqMan® assays and TaqMan Gene Expression Master Mix (Applied Biosystems, Foster City, USA). The 2<sup>-ΔΔCT</sup> method was used to validate the gene expression. Data were normalized to *Gapdh* and wt naïve or wt crush rats. 7 wt and 6 ΔETorA nerve-injured rats treated with a standard chow diet, and 9 wt and 8 ΔETorA nerve-injured rats treated with fenofibrate were included into qPCR analyses.

### 2.9. <sup>18</sup>F-fluorodeoxyglucose autoradiography

<sup>18</sup>F-fluorodeoxyglucose (<sup>18</sup>F-FDG) (37 MBq) was injected intraperitoneally 60 min before euthanasia. Frozen brains were cut into 20-μm coronal slices. Slices were exposed against imaging plates for 60 min and images were acquired with the CR 35 Bio high-speed scanner (Raytest, Straubenhardt, Germany). For the quantification of <sup>18</sup>F-FDG uptake distribution, intensity measurements of triplicates for each region of interests (ROIs) per animal were performed. ROIs were set on striatum, primary motor cortex, somatosensory cortex, thalamus, SN, and cerebellar lobule according to the rat stereotaxic atlas (Paxinos and Watson, 2007). After subtraction of the background, the data were normalized to the reference corpus callosum and presented as <sup>18</sup>F-FDG uptake ratio. 7 naïve wt, 9 naïve ΔETorA, 9 nerve-injured wt, and 10 nerve-injured ΔETorA rats were included into <sup>18</sup>F-FDG autoradiography analyses.

### 2.10. Statistics

Statistical analysis was performed by using GraphPad Prism software (Version 10; San Diego, CA, USA). The distribution of data was investigated via Kolmogorow-Smirnow normality test. For multiple comparisons of nonparametric data, the Kruskal–Wallis test with Dunn’s multiple comparison test was performed and for normally distributed data one-way ANOVA with Tukey’s multiple comparison test was used. Single comparisons of nonparametric data were assessed by Mann–Whitney test. Results are shown as mean ± standard error of mean (SEM). Differences are reported significant at *p* < 0.05 (\**p* < 0.05, \*\**p* < 0.01).

3. Results

3.1. *ΔETorA* rats are highly susceptible to peripheral nerve injury-induced gene expression changes in the striatum

To obtain broader insights into the molecular pathophysiology of DLM development, we isolated striatal tissue contralateral to the nerve-injured side in naïve and nerve-crushed wt and *ΔETorA* rats twelve weeks after trauma and performed RNA-seq. Comparing either wt naïve with *ΔETorA* naïve rats or nerve-injured *ΔETorA* (*ΔETorA* crush) with nerve-injured wt (wt crush) rats yielded only a low number of DEGs with 17 and 26, respectively (Fig. 1A, supplementary material 1 -

Supplemental Fig. 1, supplementary material 2). In contrast, the *ΔETorA* crush group displayed the highest number of 1009 DEGs over naïve *ΔETorA* rats, while wt crush and wt naïve rats differed only in 216 DEGs. Comparison between *ΔETorA* crush and wt naïve rats resulted in 170 DEGs. These data demonstrate that the *ΔETorA* mutation itself results in only minor molecular changes in naïve animals while at the same time conveying a high susceptibility to transcriptomic alteration induced by peripheral nerve injury.

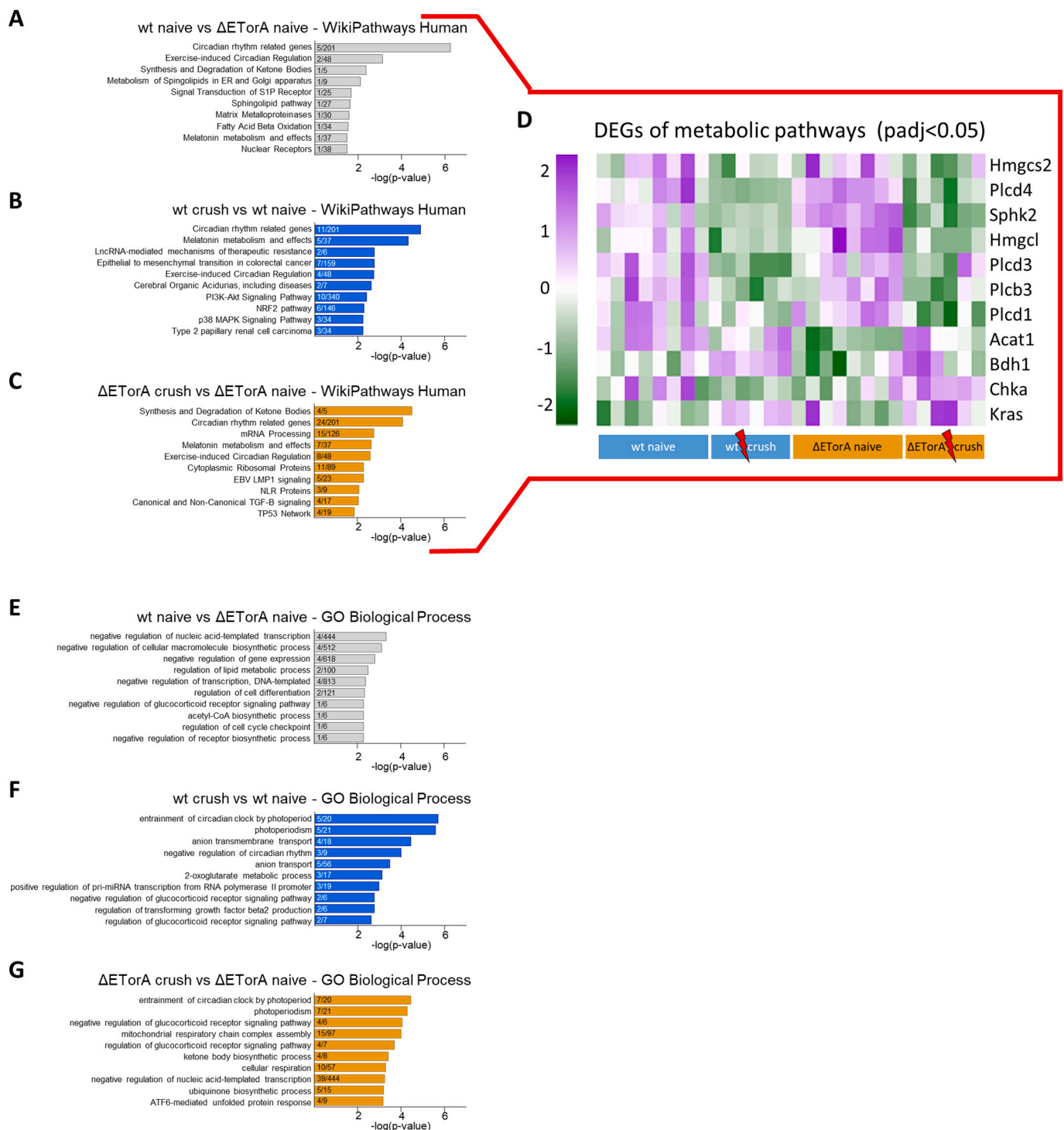


Fig. 1. Overview of differentially expressed genes (DEGs) of *ΔETorA* and wt rats with and without nerve crush injury identified by RNA-seq in the striatum. RNA-seq analysis in the contralateral striatum twelve weeks after sciatic nerve crush and in naïve state by a two-group comparison between wt naïve, wt crush, *ΔETorA* naïve, and *ΔETorA* crush rats (n = 6–8). Illustration shows the number of total, up-regulated or down-regulated DEGs of each comparison group (A). 3-way venn diagram shows the number of overlapping total DEGs of the comparison groups wt naïve vs *ΔETorA* naïve, *ΔETorA* crush vs *ΔETorA* naïve, wt crush vs wt naïve (n = 6–8) (B). Used cutoff criteria: padj: 0.05.

### 3.2. Genotype- and phenotype-dependent effect on energy metabolism pathways in the striatum

Focusing on naïve rats and on the genotype-dependent effect of nerve injury we identified seven overlapping genes in total (Fig. 1B, supplementary material 3). These consisted of *Dpd*, *Nr1d1*, *Nr1d2*, *Ciart*,

*Klhdc7a*, *Mmp14*, *Sphk2*, genes that are involved in glucose and lipid metabolism as well as in regulation of the circadian rhythm. Additionally, gene set enrichment analysis of total DEGs was performed by using the webserver Enrichr for the analysis of regulated pathways with the gene set library WikiPathways 2019 Human (Fig. 2A-C, supplementary material 4) and the Gene Ontology (GO) terms for biological processes



**Fig. 2.** Top enriched pathways and gene ontology (GO) terms underlying biological processes in the striatum of  $\Delta$ ETorA and wt rats with and without nerve crush injury.

Enrichment analysis for WikiPathways 2019 Human pathways (A to C) and GO Biological Process 2018 (E to G) terms of the striatum by a two-group comparison between wt naïve vs  $\Delta$ ETorA naïve,  $\Delta$ ETorA crush vs  $\Delta$ ETorA naïve, wt crush vs wt naïve ( $n = 6-8$ ). Used cutoff criteria: padj: 0.05; log2FC: 0.00. Heatmap of DEGs from metabolic pathways selected from the top ten enriched WikiPathways 2019 Human pathway terms of the comparison groups wt naïve vs  $\Delta$ ETorA naïve,  $\Delta$ ETorA crush vs  $\Delta$ ETorA naïve, wt crush vs wt naïve, which are involved in energy metabolism (D).

(Fig. 2E-G, supplementary material 4). The total numbers of regulated pathways ( $p < 0.05$ ) as well as a detailed list of enriched pathways for each comparison group of WikiPathways 2019 Human and GO Biological Process 2018 are shown in supplementary material 1 - Supplemental Fig. 2 and supplementary material 4. Comparing naïve wt to naïve  $\Delta$ ETorA rats showed a strong genotype-dependent effect on pathways of circadian rhythm related genes and genes involved in the energy metabolism (Fig. 2A, supplementary material 4). Energy metabolism pathways were also involved by comparing wt crush to wt naïve animals (Fig. 2B, supplementary material 4) and  $\Delta$ ETorA crush with  $\Delta$ ETorA naïve rats (Fig. 2C, supplementary material 4). Across all pairwise comparisons, pathways of the energy metabolism consisted of terms such as “Fatty Acid Beta Oxidation”, “Synthesis and Degradation of Ketone Bodies”, “Metabolism of Sphingolipids in ER and Golgi apparatus”, “Sphingolipid pathway”, “Signal Transduction of S1P Receptor”, “Mitochondrial LC-Fatty Acid Beta-Oxidation”, “Globo sphingolipid metabolism”, and “Nuclear Receptors in Lipid Metabolism and Toxicity”. Specifically, DEGs from Top Ten enriched pathways related to energy metabolism were *Sphk2*, *Hmgcs2*, *Hmgcl*, *Bdh1*, *Acat1*, *Kras*, *Chka*, *Plcd1*, *Plcd3*, *Plcd4*, *Plcb3* (Fig. 2D). Also the analysis of GO for biological processes showed terms belonging to the energy metabolism (Fig. 2E-G, supplementary material 4).

Since torsins are known as essential regulators of cellular lipid

metabolism (Grillet et al., 2016), we focused on genes involved in fatty acid  $\beta$ -oxidation, a process involving multiple steps to break down fatty acid molecules to produce energy. Indeed, we found various genes that are expressed by mitochondria or peroxisomes that were involved in  $\beta$ -oxidation and were reduced in wt rats after nerve injury compared to naïve littermates. These genes comprise *Acaa1b*, *Acacb*, *Acadm*, *Cpt1a*, and *Pex11a* (Fig. 3A-F). Interestingly, this reduction of gene expression did not occur in  $\Delta$ ETorA rats after nerve injury (Fig. 3B-F), thereby pointing towards transcriptional alterations of the energy metabolism in  $\Delta$ ETorA rats that becomes evident after a stressful event.

### 3.3. Nerve injury leads to increased brain glucose uptake in cortex and striatum

Energy supply to the brain depends mostly on glucose consumption. We therefore addressed the question whether peripheral nerve injury might influence brain glucose metabolism in rats. For this, we performed  $^{18}\text{F}$ -FDG autoradiography. The glucose uptake in the motor cortex, sensory cortex, and striatum showed increased glucose metabolism in both nerve-injured wt and  $\Delta$ ETorA rats, albeit slightly lower in nerve-injured  $\Delta$ ETorA rats. Additionally, in naïve  $\Delta$ ETorA rats, glucose uptake was slightly elevated, though not significantly, in these brain regions compared to naïve wt rats (Fig. 4). This data once again suggests

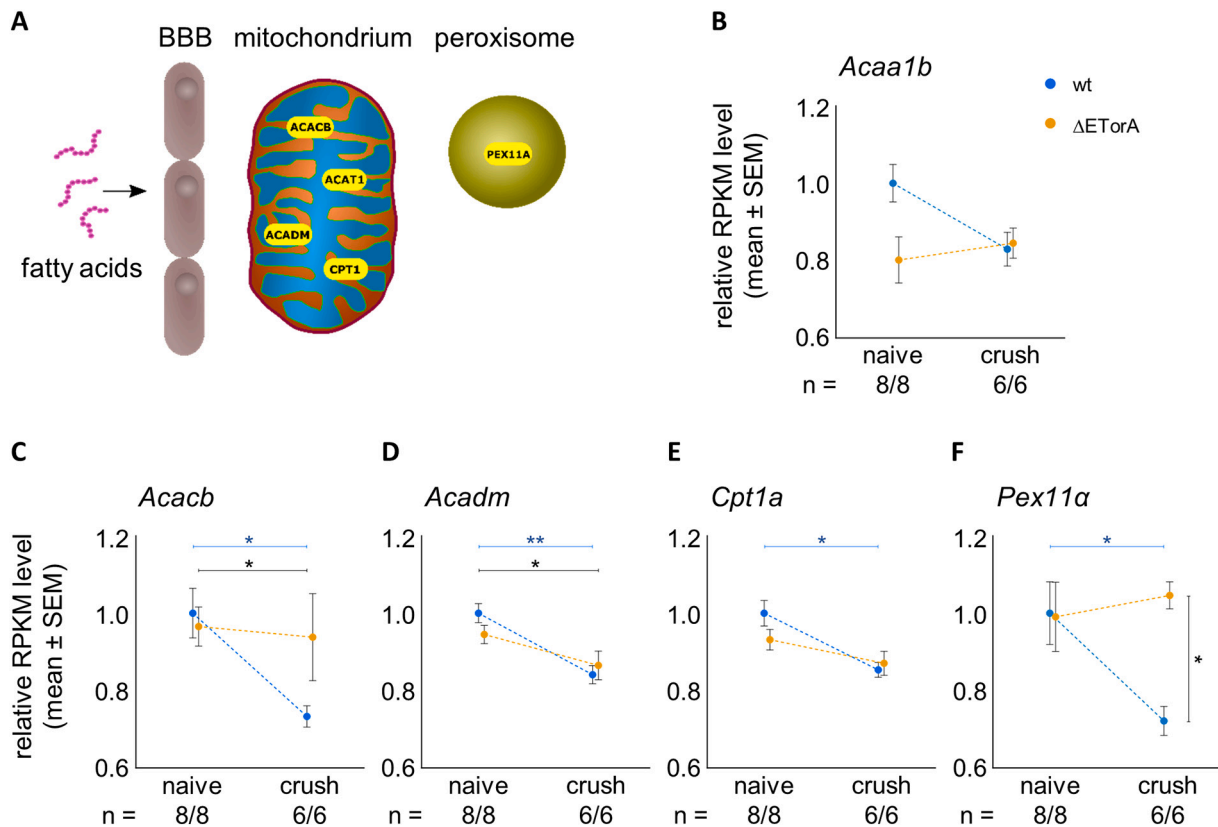


**Fig. 3.** Regulated genes of the energy metabolism in the striatum after nerve crush injury.

Illustration of selected genes involved in  $\beta$ -oxidation (A). Expression levels in the striatum of fatty acid  $\beta$ -oxidation-related genes (B) acetyl-Coenzyme A acyltransferase 1B (*Acaa1b*;  $H$ : 7.97,  $p < 0.05$ ; pairwise comparison: no significant differences; mean  $\pm$  SEM: wt naïve (1.00  $\pm$  0.05),  $\Delta$ ETorA naïve (0.80  $\pm$  0.06), wt crush (0.83  $\pm$  0.04),  $\Delta$ ETorA crush (0.85  $\pm$  0.04)), (C) acetyl-CoA carboxylase beta (*Acacb*;  $H$ : 10.24,  $p < 0.05$ ; pairwise comparison: wt naïve vs wt crush ( $p = 0.0182$ ),  $\Delta$ ETorA naïve vs wt crush ( $p = 0.0439$ ); mean  $\pm$  SEM: wt naïve (1.00  $\pm$  0.06),  $\Delta$ ETorA naïve (0.97  $\pm$  0.05), wt crush (0.733  $\pm$  0.03),  $\Delta$ ETorA crush (0.94  $\pm$  0.11)), (D) acyl-CoA dehydrogenase medium chain (*Acadm*;  $H$ : 12.96,  $p < 0.01$ ; pairwise comparison: wt naïve vs wt crush ( $p = 0.0094$ ), wt naïve vs  $\Delta$ ETorA crush ( $p = 0.0451$ ); mean  $\pm$  SEM: wt naïve (1.00  $\pm$  0.02),  $\Delta$ ETorA naïve (0.95  $\pm$  0.02), wt crush (0.84  $\pm$  0.02),  $\Delta$ ETorA crush (0.87  $\pm$  0.04)), (E) carnitine palmitoyltransferase 1 A (*Cpt1a*;  $H$ : 9.56,  $p < 0.05$ ; pairwise comparison: wt naïve vs wt crush ( $p = 0.0303$ ); mean  $\pm$  SEM: wt naïve (1.00  $\pm$  0.03),  $\Delta$ ETorA naïve (0.93  $\pm$  0.03), wt crush (0.85  $\pm$  0.02),  $\Delta$ ETorA crush (0.87  $\pm$  0.03)), (F) peroxisomal biogenesis factor 11  $\alpha$  (*Pex11a*;  $H$ : 10.79,  $p < 0.05$ ; pairwise comparison: wt naïve vs wt crush ( $p = 0.0403$ ), wt crush vs  $\Delta$ ETorA crush ( $p = 0.0240$ ); mean  $\pm$  SEM: wt naïve (1.00  $\pm$  0.08),  $\Delta$ ETorA naïve (0.99  $\pm$  0.09), wt crush (0.72  $\pm$  0.04),  $\Delta$ ETorA crush (1.05  $\pm$  0.04)) revealed by RNA-seq analysis comparing wt and  $\Delta$ ETorA rats in naïve and crush state. Data are normalized to wt naïve rats ( $n = 6-8$ ). Data are shown as mean  $\pm$  SEM. Statistical analysis was performed using Kruskal-Wallis test with Dunn's multiple comparisons test. \*  $p < 0.05$ ; \*\*  $p < 0.01$ .

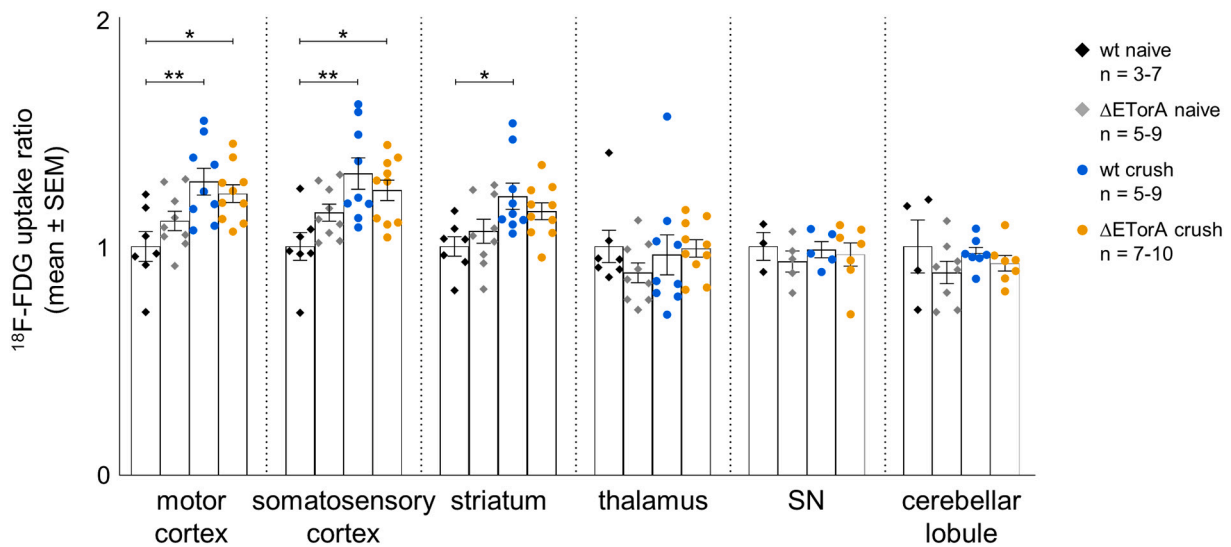


**Fig. 4.** Nerve crush injury contributes to an increase of the glucose metabolism in the central nervous system. Glucose uptake levels revealed by in vivo  $^{18}\text{F}$ -FDG autoradiography in the contralateral motor cortex ( $F_{3,31} = 5.82$ ,  $p < 0.01$ ; pairwise comparison: wt naïve vs wt crush ( $p = 0.0035$ ), wt naïve vs  $\Delta\text{ETorA}$  crush ( $p = 0.0178$ ); mean  $\pm$  SEM: wt naïve ( $1.00 \pm 0.06$ ),  $\Delta\text{ETorA}$  naïve ( $1.11 \pm 0.04$ ), wt crush ( $1.28 \pm 0.06$ ),  $\Delta\text{ETorA}$  crush ( $1.23 \pm 0.04$ )), somatosensory cortex ( $F_{3,31} = 5.965$ ,  $p < 0.01$ ; pairwise comparison: wt naïve vs wt crush ( $p = 0.0020$ ), wt naïve vs  $\Delta\text{ETorA}$  crush ( $p = 0.0182$ ); mean  $\pm$  SEM: wt naïve ( $1.00 \pm 0.06$ ),  $\Delta\text{ETorA}$  naïve ( $1.15 \pm 0.04$ ), wt crush ( $1.32 \pm 0.07$ ),  $\Delta\text{ETorA}$  crush ( $1.25 \pm 0.04$ )), striatum ( $F_{3,31} = 3.744$ ,  $p < 0.05$ ; pairwise comparison: wt naïve vs wt crush ( $p = 0.0225$ ); mean  $\pm$  SEM: wt naïve ( $1.00 \pm 0.04$ ),  $\Delta\text{ETorA}$  naïve ( $1.07 \pm 0.05$ ), wt crush ( $1.22 \pm 0.06$ ),  $\Delta\text{ETorA}$  crush ( $1.15 \pm 0.04$ )), thalamus (mean  $\pm$  SEM: wt naïve ( $1.00 \pm 0.07$ ),  $\Delta\text{ETorA}$  naïve ( $0.89 \pm 0.04$ ), wt crush ( $0.96 \pm 0.09$ ),  $\Delta\text{ETorA}$  crush ( $0.99 \pm 0.04$ )), SN (mean  $\pm$  SEM: wt naïve ( $1.00 \pm 0.06$ ),  $\Delta\text{ETorA}$  naïve ( $0.93 \pm 0.05$ ), wt crush ( $0.99 \pm 0.03$ ),  $\Delta\text{ETorA}$  crush ( $0.97 \pm 0.05$ )), and cerebellar lobule (mean  $\pm$  SEM: wt naïve ( $1.00 \pm 0.12$ ),  $\Delta\text{ETorA}$  naïve ( $0.89 \pm 0.05$ ), wt crush ( $0.97 \pm 0.3$ ),  $\Delta\text{ETorA}$  crush ( $0.93 \pm 0.03$ )) of wt and  $\Delta\text{ETorA}$  rats in naïve and crush state ( $n = 3-10$ ). Data are normalized to corpus callosum and wt naïve rats. Data are shown as mean  $\pm$  SEM. Statistical analysis was performed using One-way ANOVA with Tukey's multiple comparisons test. \*  $p < 0.05$ ; \*\*  $p < 0.01$ .

alterations in an additional contributor to the energy metabolism in DYT-TOR1A dystonia. No differences in the glucose metabolism of the thalamus, SN, and cerebellar lobule were detected.

### 3.4. $\Delta\text{ETorA}$ rats demonstrate alterations of genes involved in the brain energy metabolism

Genes of the fatty acid  $\beta$ -oxidation, which showed genotype-dependent changes after nerve crush injury (Fig. 3), are mostly regulated by the master regulator PPAR $\alpha$  (Kersten, 2014). PPAR $\alpha$  is a ligand-activated transcription factor, which serves as regulator of energy metabolism processes.

To determine if the energy metabolism and specifically PPAR $\alpha$  indeed has an impact on the pathophysiology of DYT-TOR1A dystonia, we challenged nerve-injured wt and  $\Delta\text{ETorA}$  rats with the PPAR $\alpha$  agonist fenofibrate. These rats were fed with fenofibrate-containing chow (or standard chow) for nine weeks, starting three weeks after the nerve crush injury. Analysis of the mRNA level of the mutated human DYT-TOR1A showed a significant reduction after fenofibrate treatment, thus pointing towards a direct interaction of PPAR $\alpha$  and the mutated DYT-TOR1A gene (Fig. 5A).

As expected, fenofibrate treatment in both wt and  $\Delta\text{ETorA}$  rats increased levels of PPAR $\alpha$ -dependent mRNAs in the liver, where PPAR $\alpha$  is predominantly expressed, such as *Pex11a*, *Fgf21*, and *Pfk4*, thereby demonstrating a positive target engagement of fenofibrate administration (supplementary material 1 - Supplemental Fig. 3). To assess the pharmacological effect of fenofibrate in the brain of wt and  $\Delta\text{ETorA}$  rats, we measured mRNA levels of *Acaa1b*, *Acacb*, *Acadm*, *Cpt1a*, and *Pex11a* in brain tissue. Contrasting the observation made from liver tissue, fenofibrate treatment over nine weeks in wt rats decreased the mRNA levels of *Acacb* and *Cpt1a* significantly, while *Acaa1b*, *Acadm*, and *Pex11a* levels were reduced but did not reach significance (Fig. 5B). In contrast, this reduction was not found in *Acacb*, *Acadm*, *Cpt1a*, and *Pex11a* of  $\Delta\text{ETorA}$  rats. These results emphasize the alterations in gene transcription related to crucial participants in brain energy metabolism

within the brains of  $\Delta\text{ETorA}$  rats.

### 3.5. PPAR $\alpha$ agonist treatment modulates dystonia-like movements in nerve crush injured rats

To functionally assess the effect of PPAR $\alpha$  modulation on the dystonic phenotype, we analyzed tail suspension video recordings of crush-injured wt and  $\Delta\text{ETorA}$  rats fed with either fenofibrate-containing chow or control standard chow. Using deep-learning based kinematic analyses we identified increased coherence and directed connectivity (TPDC) of the nerve-injured right hind limb in fenofibrate treated over untreated wt rats (supplementary material 1 - Supplemental Fig. 5, supplementary video S1). This reflects a higher level of involuntary and synchronized movements of the right hind limb, a measure for DLM, already in nerve-injured wt rats (Fig. 6A,B,E,F).  $\Delta\text{ETorA}$  rats receiving control chow showed the highest coherence and TPDC values and thereby presented the most severe DLM (Fig. 6C,E,F) whereas fenofibrate therapy reduced DLM nearly to untreated wt levels (Fig. 6D,E,F). In contrast to these outcomes, the analyses conducted on the uninjured left hind limb did not reveal any substantial alterations in terms of coherence and TPDC comparing all four groups of rats (supplementary material 1 - Supplemental Fig. 4). The elevated coherence and increased TPDC of the right hind limb exhibited by the two groups - fenofibrate-treated wt rats (Fig. 6B) and control chow-treated  $\Delta\text{ETorA}$  rats (Fig. 6C) - manifested in a modular organization that was remarkably similar, characterized by two modules for coherence and for directed connectivity. This suggests a heightened integrated and synchronized connectivity pattern among the markers. Conversely, only in the control chow-treated wt rats (Fig. 6A), three modules were identified, indicating a more distributed and less organized marker arrangement within the hindlimb, indicative for a more physiological state. These findings imply that the well-integrated modular arrangement and enhanced synchronization observed in the right hind limb of rats after nerve injury are indicative of static and involuntary DLM. Intriguingly, fenofibrate-treated  $\Delta\text{ETorA}$  rats (Fig. 6D) also exhibited two modules, pointing towards an incomplete

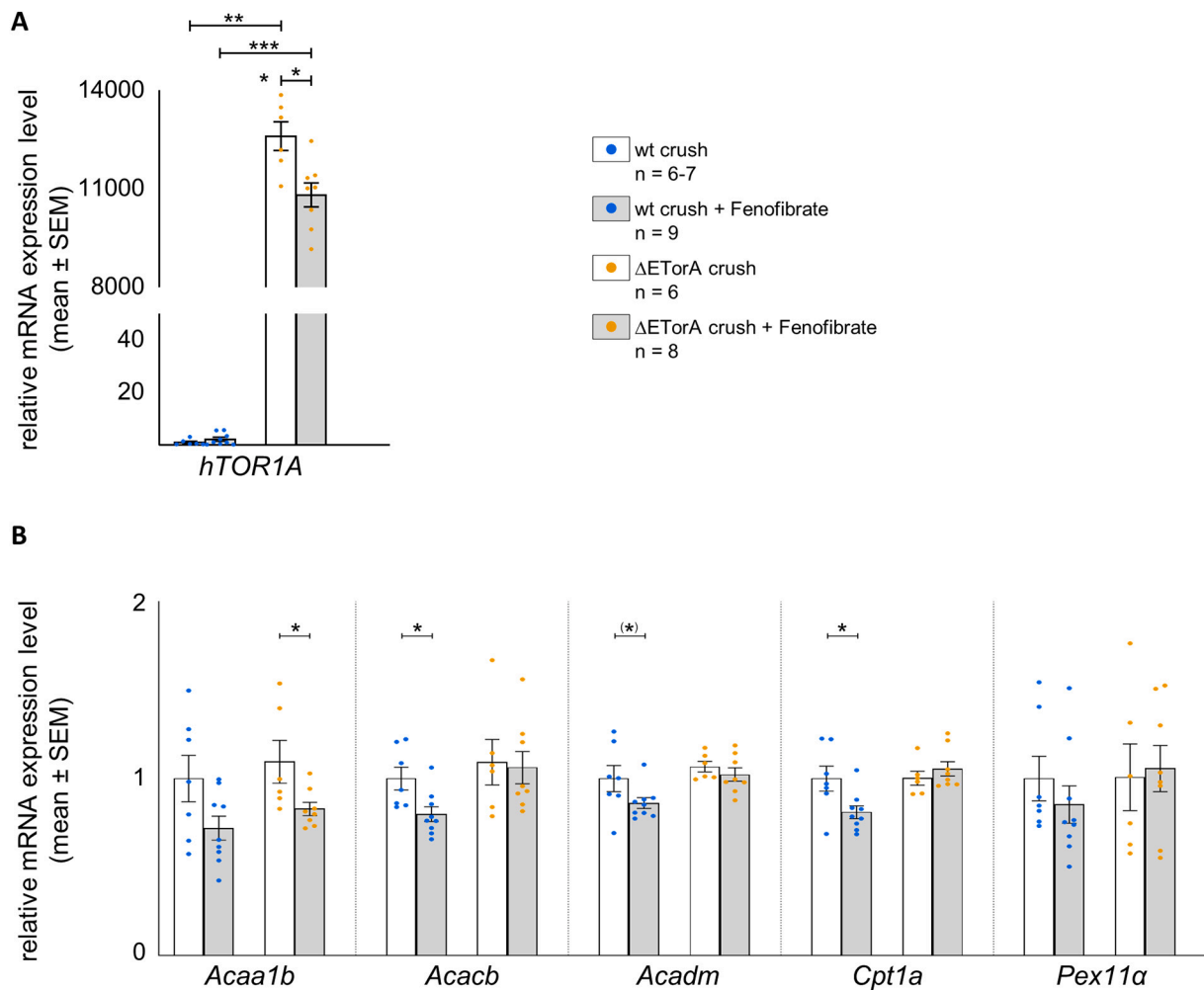


**Fig. 5.** Treatment with fenofibrate reduces gene expression of energy metabolism related genes in the striatum of nerve-injured wt animals.

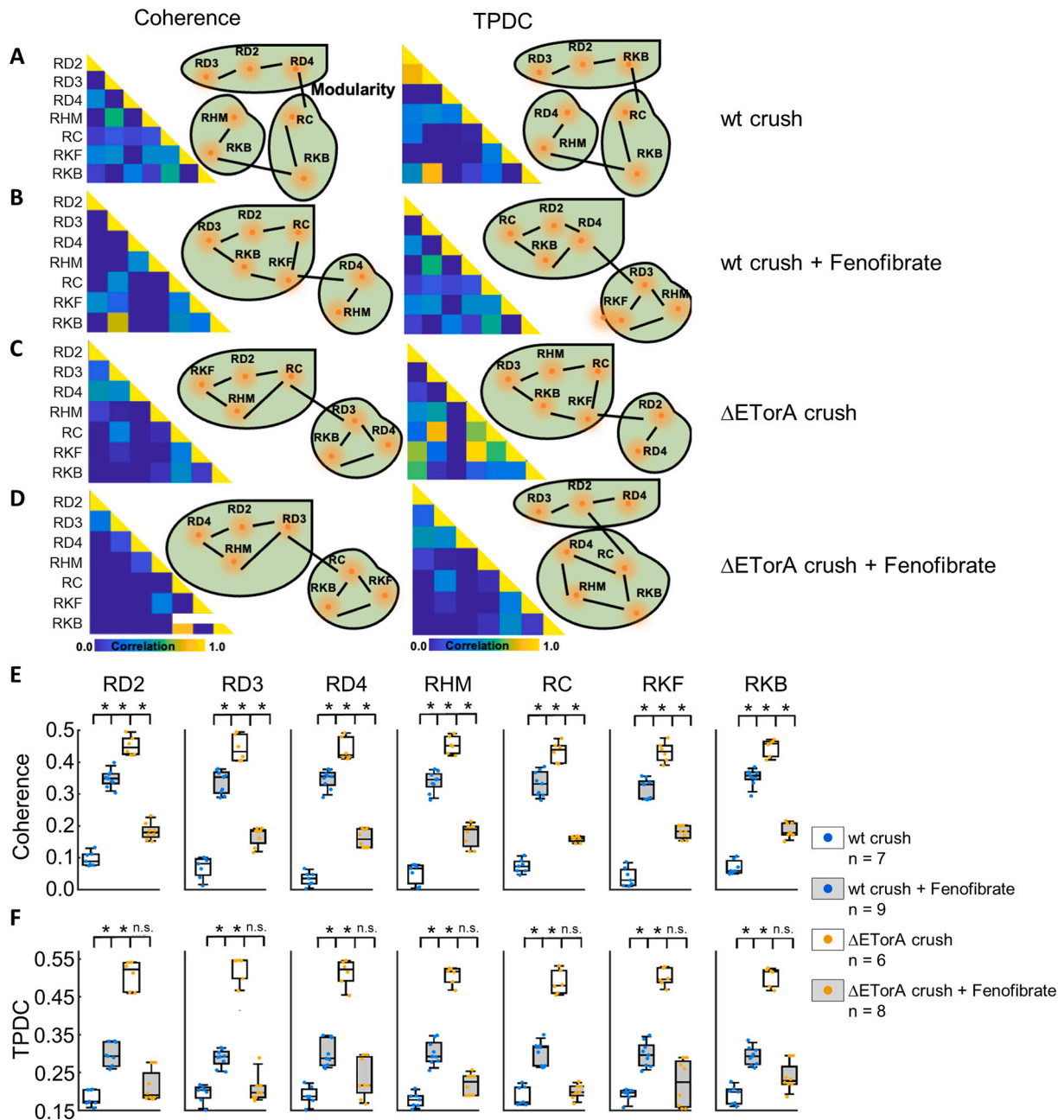
Regulation of gene expression in the striatum after nine weeks of fenofibrate treatment of nerve-injured wt and ΔETorA rats revealed by qPCR. Relative mRNA gene expression levels of the human mutated *TOR1A* gene (A) (ΔETorA crush vs ΔETorA crush + Fenofibrate ( $p = 0.0127$ ), wt crush + Fenofibrate vs ΔETorA crush + Fenofibrate ( $p < 0.0001$ ); mean ± SEM: wt crush ( $1.00 \pm 0.46$ ), wt crush + Fenofibrate ( $2.21 \pm 0.75$ ), ΔETorA crush ( $12,616 \pm 437$ ), ΔETorA crush + Fenofibrate ( $10,824 \pm 366$ )) and genes involved in energy metabolism of the fatty acid β-oxidation (B) (*Acaa1b*: ΔETorA crush vs ΔETorA crush + Fenofibrate ( $p = 0.0426$ ); mean ± SEM: wt crush ( $1.00 \pm 0.13$ ), wt crush + Fenofibrate ( $0.72 \pm 0.07$ ), ΔETorA crush ( $1.10 \pm 0.12$ ), ΔETorA crush + Fenofibrate ( $0.83 \pm 0.04$ ) / *Acacb*: wt crush vs wt crush + Fenofibrate ( $p = 0.0164$ ); mean ± SEM: wt crush ( $1.00 \pm 0.07$ ), wt crush + Fenofibrate ( $0.80 \pm 0.04$ ), ΔETorA crush ( $1.09 \pm 0.13$ ), ΔETorA crush + Fenofibrate ( $1.06 \pm 0.09$ ) / *Acadm*: wt crush vs wt crush + Fenofibrate ( $p = 0.0549$ ); mean ± SEM: wt crush ( $1.00 \pm 0.07$ ), wt crush + Fenofibrate ( $0.86 \pm 0.03$ ), ΔETorA crush ( $1.07 \pm 0.03$ ), ΔETorA crush + Fenofibrate ( $1.02 \pm 0.04$ ) / *Cpt1a*: wt crush vs wt crush + Fenofibrate ( $p = 0.0418$ ); mean ± SEM: wt crush ( $1.00 \pm 0.07$ ), wt crush + Fenofibrate ( $0.81 \pm 0.04$ ), ΔETorA crush ( $1.00 \pm 0.04$ ), ΔETorA crush + Fenofibrate ( $1.06 \pm 0.04$ ) / *Pex11a*: mean ± SEM: wt crush ( $1.00 \pm 0.13$ ), wt crush + Fenofibrate ( $0.85 \pm 0.10$ ), ΔETorA crush ( $1.00 \pm 0.19$ ), ΔETorA crush + Fenofibrate ( $1.06 \pm 0.13$ )) by comparing nerve-injured wt and ΔETorA rats with and without fenofibrate treatment ( $n = 6-9$ ). Data are normalized to *Gapdh* and wt crush rats. Data are shown as mean ± SEM. Statistical analysis was performed using Mann Whitney test. (\*)  $p = 0.0549$ ; \*  $p < 0.05$ ; \*\*  $p < 0.01$ ; \*\*\*\*  $p < 0.0001$ .

reduction of DLM by this intervention. These results provide evidence that the manipulation of PPARα activity leads to distinct effects on DLM in wt and ΔETorA rats, thereby pointing towards a role of PPARα in the symptomatogenesis of dystonic movements.

#### 4. Discussion

In the present study, we employed RNA-sequencing on striatal tissue in the ΔETorA dystonia rat model that exhibits DLM and adheres to the “second hit” hypothesis (Knorr et al., 2021). This hypothesis postulates that the symptomatic manifestation of a dystonic movement disorders depends on the interplay between intrinsic (genetic) predisposition and a maladaptive response of basal-ganglia motor circuits to a sensorimotor stressor. We revealed an array of DEGs and uncovered novel potential pathways that may contribute to the underlying pathophysiology of dystonia. The degree of genetic variability between wt and ΔETorA rats

in their naïve state was found to be minimal within the striatal tissue, with 17 DEGs identified. Nevertheless, it is crucial to acknowledge that not all changes manifest at the mRNA level. Endophenotypic alterations are present across the entire spectrum, from molecular to systemic network levels, even in non-manifesting DYT-TOR1A gene carriers. Additionally, analyzing the entire striatum, composed of diverse cell types, may fail to detect subtle cell type-specific effects in such an analysis. However, the sciatic nerve crush injury exerted a substantial influence on gene expression within the striatum. Notably, this modulation was more pronounced in rats bearing a transgenic dystonia background (ΔETorA) with 1009 DEGs compared to those with a wt background with 216 DEGs. The genotype-dependent transcriptomic changes in the central nervous system (CNS) following peripheral nerve crush injury underscore the pivotal role of peripheral trauma as a sensorimotor stressor affecting striatal neuronal activity and corroborates previous findings from various human studies, that dystonia is



RD2-4: second to fourth digit tip, RHM: right hand mid, RC: right calcaneus, RKF: right knee front, RKB: right knee back

**Fig. 6.** Coherence, directed connectivity and modularity.

The correlation matrices of coherence and of directed connectivity (TPDC) for the four groups ( $n = 6-9$ ) wt crush (A), wt crush with fenofibrate treatment (B),  $\Delta$ ETorA crush (C) and  $\Delta$ ETorA crush with fenofibrate treatment (D). The individual coherence values for the four groups are shown in (E) (mean  $\pm$  SEM of wt crush, wt crush + Fenofibrate,  $\Delta$ ETorA crush,  $\Delta$ ETorA crush + Fenofibrate: RD2 ( $0.096 \pm 0.008$ ,  $0.348 \pm 0.009$ ,  $0.452 \pm 0.012$ ,  $0.183 \pm 0.009$ ), RD3 ( $0.112 \pm 0.011$ ,  $0.354 \pm 0.011$ ,  $0.449 \pm 0.015$ ,  $0.201 \pm 0.009$ ), RD4 ( $0.080 \pm 0.007$ ,  $0.362 \pm 0.009$ ,  $0.446 \pm 0.013$ ,  $0.195 \pm 0.009$ ), RHM ( $0.096 \pm 0.011$ ,  $0.355 \pm 0.010$ ,  $0.459 \pm 0.010$ ,  $0.205 \pm 0.012$ ), RC ( $0.116 \pm 0.007$ ,  $0.348 \pm 0.012$ ,  $0.440 \pm 0.012$ ,  $0.193 \pm 0.003$ ), RKF ( $0.085 \pm 0.010$ ,  $0.335 \pm 0.009$ ,  $0.439 \pm 0.012$ ,  $0.213 \pm 0.006$ ), RKB ( $0.113 \pm 0.008$ ,  $0.368 \pm 0.008$ ,  $0.452 \pm 0.010$ ,  $0.217 \pm 0.007$ )) and the TPDC values are depicted in (F) (mean  $\pm$  SEM of wt crush, wt crush + Fenofibrate,  $\Delta$ ETorA crush,  $\Delta$ ETorA crush + Fenofibrate: RD2 ( $0.183 \pm 0.008$ ,  $0.296 \pm 0.010$ ,  $0.508 \pm 0.015$ ,  $0.212 \pm 0.015$ ), RD3 ( $0.195 \pm 0.009$ ,  $0.288 \pm 0.008$ ,  $0.525 \pm 0.014$ ,  $0.207 \pm 0.013$ ), RD4 ( $0.188 \pm 0.009$ ,  $0.300 \pm 0.012$ ,  $0.513 \pm 0.014$ ,  $0.234 \pm 0.019$ ), RHM ( $0.177 \pm 0.007$ ,  $0.302 \pm 0.010$ ,  $0.507 \pm 0.010$ ,  $0.219 \pm 0.010$ ), RC ( $0.188 \pm 0.010$ ,  $0.303 \pm 0.010$ ,  $0.488 \pm 0.013$ ,  $0.199 \pm 0.007$ ), RKF ( $0.191 \pm 0.006$ ,  $0.298 \pm 0.011$ ,  $0.501 \pm 0.010$ ,  $0.221 \pm 0.022$ ), RKB ( $0.190 \pm 0.009$ ,  $0.293 \pm 0.008$ ,  $0.504 \pm 0.010$ ,  $0.238 \pm 0.013$ )). Statistical analysis was performed using Mann Whitney test \*  $p < 0.0001$ , not significant (n.s.)  $p > 0.05$ .

related to maladaptive striatal dysfunction (Jankovic, 2009; Jankovic and Van der Linden, 1988; Kumar and Jog, 2011; Macerollo et al., 2019; Sheehy and Marsden, 1980). Furthermore, the high number of 1009 DEGs in the comparison between naïve  $\Delta$ ETorA and nerve-injured  $\Delta$ ETorA rats underscores the impact of the “second hit” concept of

gene-environment interaction in our transgenic DYT-TOR1A dystonia rodent model.

The enrichment analysis of DEGs in the striatum revealed multiple dysregulated pathways. Notably, many pathways implicated in our transcriptome data are closely associated with the energy metabolism.

Interestingly, although the brain represents only 2% of the body's mass, it consumes 20% of the overall body energy requirement, with glucose serving as the predominant source of energy supply (Kety, 1957; Mink et al., 1981; Sokoloff, 1960). Additionally, lactate, ketone bodies, and fatty acids act as supplementary substrates for energy metabolism (Belanger et al., 2011; Nehlig, 2004; van Hall et al., 2009). These substrates ultimately convert to pyruvate and subsequently to acetyl-CoA, which enters the metabolic pathway of the tricarboxylic acid (TCA) cycle in mitochondria, providing adenosine triphosphate (ATP) as source of energy (Romano et al., 2017).

Given the established role of torsins as regulators of cellular lipid metabolism (Grillet et al., 2016), we focused our attention on genes involved in fatty acid  $\beta$ -oxidation. Fatty acids play a crucial role in energy metabolism, belonging to the lipid category, which encompasses triacylglycerols, phospholipids, sterol lipids, and sphingolipids. The liver and adipose tissue produce fatty acids, which are transported across the blood-brain barrier (BBB) by fatty acid transport proteins and are taken up mainly by glial cells in the CNS (Mitchell et al., 2011; Schonfeld and Reiser, 2013). Mitochondria and peroxisomes serve as important organelles for fatty acid metabolism, contributing to energy generation through  $\beta$ -oxidation by breaking down long-chain fatty acids to acetyl-CoA (Romano et al., 2017; Wanders et al., 2003). The energy metabolism of fatty acids is associated with functions related to repair processes, neurodevelopment, and neurotransmission (Schonfeld and Reiser, 2013). Ketone bodies, including acetoacetate, 3-hydroxybutyrate, and acetone, act as alternative energy sources for brain neurons and glial cells when glucose availability is insufficient, as seen during prolonged fasting or in the early stages of maturation. Primarily derived from fatty acids in the liver, they are transported across the BBB by monocarboxylate transporters. The attributed functions of ketone bodies encompass neuroprotection and the synthesis of lipids (Morris, 2005).

Glucose metabolism plays a crucial role in brain physiology, a facet we explored through  $^{18}\text{F}$ -FDG autoradiography in our  $\Delta\text{ETorA}$  dystonia rat model. Our findings indicate a physiological surge in glucose uptake in the brains of wt rats subjected to nerve injury, a response that appears less robust in  $\Delta\text{ETorA}$  rats. From this, we infer heightened activity in these brain regions in wt rats post-peripheral nerve injury. Yet, we cannot definitively ascertain whether this discrepancy implies a lack of compensatory mechanisms in  $\Delta\text{ETorA}$  rats for a potentially necessary increase in synaptic activity after nerve injury, or if it suggests inadequate and untimely glucose availability in  $\Delta\text{ETorA}$  rats. Previous studies have also noted altered glucose activity in the lentiform nuclei, cerebellum, and supplementary motor areas in both manifesting and non-manifesting DYT-TOR1A gene carriers when compared to healthy subjects in a movement-free state (Eidelberg et al., 1998). The observed elevation in glucose activity in non-manifesting DYT-TOR1A gene carriers, considered as an endophenotype of DYT-TOR1A dystonia, is also reflected in our findings, showing a slightly increased glucose metabolism in naïve  $\Delta\text{ETorA}$  rats.

Furthermore, after nerve injury, we observed reduced expression of key  $\beta$ -oxidation genes, such as *Acaa1b*, *Acacb*, *Acadm*, *Cpt1a*, and *Pex11a*, in wt rats, but not in  $\Delta\text{ETorA}$  rats. This indicates transcriptional abnormalities in the energy metabolism of the  $\Delta\text{ETorA}$  rat brain triggered by peripheral stress. Consistent with this observation, axotomy of retinal ganglion cells was shown to elevate lipin levels, a key regulator of lipid metabolism that was found to express increased activity in human neural cells of DYT-TOR1A dystonia patients and mouse models. This hints at the intriguing possibility that an injury may yield an impact on lipid homeostasis (Yang et al., 2020). Moreover, injury seems to impact pathways related to sphingolipids, a subset of lipids integral to cellular membranes. These sphingolipids regulate fundamental cellular processes such as cell growth, differentiation, senescence, and apoptosis (Bartke and Hannun, 2009). We observed dysregulation in the gene expression patterns of sphingosine kinase-2 (SPHK2) in our dystonia model. Previous research has already associated SPHK2 with movement disorders like Parkinson's disease and Huntington's disease (Moruno-

Manchon et al., 2017; Pyszko and Strosznajder, 2014; Sivasubramanian et al., 2015). Our findings thus suggest a tantalizing possibility that implicates both SPHK2 and the wider domain of lipid metabolism in the complex pathophysiology of dystonia. Echoing this insight, the existing signaling changes in lipid metabolism further accentuates the plausible role of energy metabolism in the context of DYT-TOR1A dystonia. (Cascaho et al., 2020; Grillet et al., 2016).

In contrast to DYT-TOR1A dystonia rats, wt rats can presumably counteract an insufficient and untimely ATP supply by adjusting the compilation of energy substrates through a possible physiological process. This involves reducing  $\beta$ -oxidation and increasing glucose metabolism. The rapid ATP supply from glucose, compared to the slower ATP supply from  $\beta$ -oxidation (Schonfeld and Reiser, 2013), could potentially positively influence the pathophysiological outcome in wt animals experiencing a stressful event.

PPAR $\alpha$ , functioning as a ligand-activated transcription factor, serves as a master regulator of genes implicated in fatty acid  $\beta$ -oxidation, lipid metabolism, and energy homeostasis (van Raalte et al., 2004; Yoon, 2009). While PPAR $\alpha$  is primarily expressed in the liver, it also exhibits varying expression levels across diverse tissues such as the kidney, heart, skeletal muscle, brain, and other regions (Auboeuf et al., 1997; Braissant et al., 1996). Hypothesizing that PPAR $\alpha$  might have implications in the pathophysiology of DYT-TOR1A dystonia, we administered fenofibrate, a PPAR $\alpha$  agonist, to challenge wt and  $\Delta\text{ETorA}$  rats after nerve injury. Interestingly, in wt rats fenofibrate treatment resulted in reduced mRNA levels of several genes associated with energy metabolism such as *Acacb* and *Cpt1a*. Moreover, wt rats developed more severe DLM when treated with fenofibrate. In contrast, we observed a lack of responsiveness of nerve-injured  $\Delta\text{ETorA}$  rats to the PPAR $\alpha$  transcriptional activation hinting at a potential tissue-specific disturbance, specifically regarding the expression of genes involved in the  $\beta$ -oxidation of fatty acids. The reason why fenofibrate has no effect on these specific genes remains unclear. It is possible that the expression of the mutated *TOR1A* gene prevents alterations in the expression of these particular genes. However, we cannot precisely say whether the *TOR1A* mutation already prevents PPAR $\alpha$  transcriptional changes in these specifically involved genes in  $\Delta\text{ETorA}$  rats, as even nerve crush injury did not show alterations in gene expression. It is possible that other genes, not captured in our analysis, may be influenced by fenofibrate treatment, as PPAR $\alpha$  acts as a master regulator capable of influencing the expression of numerous target genes. Even the reduction of *hTOR1A* gene expression through fenofibrate could be a potential hypothesis for the improvement of DLM in nerve-injured  $\Delta\text{ETorA}$  rats. The outcomes observed in fenofibrate treatment could once more imply that specific pathways remain inactive due to genetic predisposition, prompting the activation of alternative pathways. However, further data are required to confirm these hypotheses. Nonetheless, fenofibrate delivery led to a partial amelioration of DLM in  $\Delta\text{ETorA}$  rats, indicating a possible therapeutic effect.

In summary, maintaining a balanced energy metabolism is crucial for the physiological activities of the brain, relying on diverse substrates. However, our transcriptional data reveals deviations in the genes related to energy metabolism in the striatal tissue of individuals with DYT-TOR1A dystonia. Complementing this, our  $^{18}\text{F}$ -FDG autoradiography data indicates variations in glucose uptake in the cortex and striatum, suggesting a potential disruption in brain energy metabolism. This disturbance could result in a shift in the utilization of energy substrates, impacting various cellular processes.

Both glucose and fatty acids play integral roles in energy metabolism, contributing to ATP production at different rates. While glucose rapidly generates ATP, ATP production through fatty acid  $\beta$ -oxidation is comparatively slower (Schonfeld and Reiser, 2013). A mismatch between energy demands and the timely provision of ATP, due to altered energy substrate compilation, may disrupt physiological brain processes. This disruption could potentially lead to neuronal hypoxia, oxidative stress, disturbed signaling, and, consequently, dystonia. Supporting this hypothesis is additional data linking DYT-TOR1A dystonia

to lipid metabolism (Cascalho et al., 2020; Grillet et al., 2016). Nevertheless, it's crucial to note that further studies are necessary to validate our hypothesis. Electrophysiological assessments and imaging technologies, including computed tomography or positron emission tomography in living animals, brain slices, or cell cultures of individuals with DYT-TOR1A dystonia and those without, could offer more precise insights into our energy metabolism hypothesis.

In conclusion, these investigations would contribute significantly to our understanding of the intricate relationship between altered energy metabolism and the manifestation of dystonia. Finally, our observation of a symptomatic effect of fenofibrate in this model is intriguing, because this drug is widely approved for the treatment of dyslipidemia and has a low toxicity profile, which may suggest the prospect of a drug repurposing study in human manifesting DYT-TOR1A carriers.

Supplementary data to this article can be found online at <https://doi.org/10.1016/j.nbd.2024.106462>.

### CRedit authorship contribution statement

**Susanne Knorr:** Writing – original draft, Visualization, Validation, Project administration, Methodology, Investigation, Formal analysis, Conceptualization. **Lisa Rauschenberger:** Writing – review & editing, Software, Investigation. **Muthuraman Muthuraman:** Writing – review & editing, Validation, Software. **Rhonda McFleder:** Writing – review & editing, Visualization. **Thomas Ott:** Writing – review & editing, Resources. **Kathrin Grundmann-Hauser:** Resources. **Takahiro Higuchi:** Writing – review & editing, Investigation. **Jens Volkmann:** Writing – review & editing, Resources, Funding acquisition. **Chi Wang Ip:** Writing – original draft, Supervision, Resources, Methodology, Funding acquisition, Conceptualization.

### Declaration of competing interest

The authors declare no competing financial interests.

### Data availability

The sequencing datasets generated and analyzed during the current study are available at GEO (<http://www.ncbi.nlm.nih.gov/geo>) under the accession number GSE249994. The experiment data that support the findings of this study are available upon request.

### Acknowledgments

This work was funded by the Deutsche Forschungsgemeinschaft (DFG, German Research Foundation) Project-ID 424778381-TRR 295 (A06 to C.W.I. and J.V.) and under the frame of EJP RD, the European Joint Programme on Rare Diseases and the European Union's Horizon 2020 research and innovation programme under the EJP RD COFUND-EJP N° 825575 (EurDyscover to J.V.), the German Federal Ministry of Education and Research (BMBF DysTract to C.W.I.), by the VERUM foundation (to C.W.I.) and by the Interdisciplinary Center for Clinical Research (IZKF) at the University of Würzburg (N-362 to C.W.I.; Z2-CSP3 to L.R.; S506 to C.W.I. and R.M.). We thank the Core Unit SysMed at the University of Würzburg for excellent technical support and RNA-seq data generation. We are grateful to Keali Röhm, Veronika Senger, Heike Menzel and Louisa Frieß for their expert technical assistance as well as Helga Brünner for the animal care.

### References

- Albanese, A., et al., 2013. Phenomenology and classification of dystonia: a consensus update. *Mov. Disord.* 28, 863–873.
- Auboeuf, D., et al., 1997. Tissue distribution and quantification of the expression of mRNAs of peroxisome proliferator-activated receptors and liver X receptor-alpha in humans: no alteration in adipose tissue of obese and NIDDM patients. *Diabetes* 46, 1319–1327.
- Augood, S.J., et al., 1998. Expression of the early-onset torsion dystonia gene (DYT1) in human brain. *Ann. Neurol.* 43, 669–673.
- Augood, S.J., et al., 1999. Distribution of the mRNAs encoding torsinA and torsinB in the normal adult human brain. *Ann. Neurol.* 46, 761–769.
- Augood, S.J., et al., 2003. Distribution and ultrastructural localization of torsinA immunoreactivity in the human brain. *Brain Res.* 986, 12–21.
- Bartke, N., Hannun, Y.A., 2009. Bioactive sphingolipids: metabolism and function. *J. Lipid Res.* 50 (Suppl), S91–S96.
- Belanger, M., et al., 2011. Brain energy metabolism: focus on astrocyte-neuron metabolic cooperation. *Cell Metab.* 14, 724–738.
- Blondel, V., et al., 2008. Fast unfolding of communities in large networks. *J. Statist. Mech. Theor. Experim.* 2008.
- Braissant, O., et al., 1996. Differential expression of peroxisome proliferator-activated receptors (PPARs): tissue distribution of PPAR-alpha, -beta, and -gamma in the adult rat. *Endocrinology* 137, 354–366.
- Cascalho, A., et al., 2020. Excess Lipin enzyme activity contributes to TOR1A recessive disease and DYT-TOR1A dystonia. *Brain* 143, 1746–1765.
- Chen, E.Y., et al., 2013. Enrichr: interactive and collaborative HTML5 gene list enrichment analysis tool. *BMC Bioinform.* 14, 128.
- Ding, H., et al., 2022. Treadmill training in Parkinson's disease is underpinned by the interregional connectivity in cortical-subcortical network. *NPJ Parkinsons Dis.* 8, 153.
- Dobin, A., et al., 2013. STAR: ultrafast universal RNA-seq aligner. *Bioinformatics* 29, 15–21.
- Edwards, M., et al., 2003. Unusual phenotypes in DYT1 dystonia: a report of five cases and a review of the literature. *Mov. Disord.* 18, 706–711.
- Eidelberg, D., et al., 1998. Functional brain networks in DYT1 dystonia. *Ann. Neurol.* 44, 303–312.
- Gioltzoglou, T., et al., 2006. Case of DYT1 dystonia triggered by bite from a moray. *Mov. Disord.* 21, 1536–1537.
- Granata, A., et al., 2008. The dystonia-associated protein torsinA modulates synaptic vesicle recycling. *J. Biol. Chem.* 283, 7568–7579.
- Grillet, M., et al., 2016. Torsins are essential regulators of cellular lipid metabolism. *Dev. Cell* 38, 235–247.
- Grundmann, K., et al., 2012. Generation of a novel rodent model for DYT1 dystonia. *Neurobiol. Dis.* 47, 61–74.
- Hanson, P.I., Whiteheart, S.W., 2005. AAA+ proteins: have engine, will work. *Nat. Rev. Mol. Cell Biol.* 6, 519–529.
- Haufe, S., et al., 2013. A critical assessment of connectivity measures for EEG data: a simulation study. *Neuroimage* 64, 120–133.
- Hewett, J., et al., 2000. Mutant torsinA, responsible for early-onset torsion dystonia, forms membrane inclusions in cultured neural cells. *Hum. Mol. Genet.* 9, 1403–1413.
- Hewett, J., et al., 2003. TorsinA in PC12 cells: localization in the endoplasmic reticulum and response to stress. *J. Neurosci.* 23, 158–168.
- Ip, C.W., et al., 2016. Tor1a+/- mice develop dystonia-like movements via a striatal dopaminergic dysregulation triggered by peripheral nerve injury. *Acta Neuropathol. Commun.* 4, 108.
- Jankovic, J., 2009. Peripherally induced movement disorders. *Neurol. Clin.* 27 (821–82), vii.
- Jankovic, J., Van der Linden, C., 1988. Dystonia and tremor induced by peripheral trauma: predisposing factors. *J. Neurol. Neurosurg. Psychiatry* 51, 1512–1519.
- Kaminski, M., Ding, M., Truccolo, W.A., Bressler, S.L., 2001. Evaluating causal relations in neural systems: granger causality, directed transfer function and statistical assessment of significance. *Biol. Cybern.* 85, 145–157.
- Kamm, C., et al., 2004. The early onset dystonia protein torsinA interacts with kinesin light chain 1. *J. Biol. Chem.* 279, 19882–19892.
- Kersten, S., 2014. Integrated physiology and systems biology of PPARalpha. *Mol. Metab.* 3, 354–371.
- Kety, S., 1957. The general metabolism of the brain *in vivo*. In: Richter, D. (Ed.), *Metabolism of the Nervous System*. Pergamon, London, pp. 221–237.
- Knorr, S., et al., 2021. The evolution of dystonia-like movements in TOR1A rats after transient nerve injury is accompanied by dopaminergic dysregulation and abnormal oscillatory activity of a central motor network. *Neurobiol. Dis.* 154, 105337.
- Kuleshov, M.V., et al., 2016. Enrichr: a comprehensive gene set enrichment analysis web server 2016 update. *Nucleic Acids Res.* 44, W90–W97.
- Kumar, H., Jog, M., 2011. Peripheral trauma induced dystonia or post-traumatic syndrome? *Can. J. Neurol. Sci.* 38, 22–29.
- Kustedjo, K., et al., 2000. Torsin A and its torsion dystonia-associated mutant forms are luminal glycoproteins that exhibit distinct subcellular localizations. *J. Biol. Chem.* 275, 27933–27939.
- Liao, Y., et al., 2014. featureCounts: an efficient general purpose program for assigning sequence reads to genomic features. *Bioinformatics* 30, 923–930.
- Love, M.I., et al., 2014. Moderated estimation of fold change and dispersion for RNA-seq data with DESeq2. *Genome Biol.* 15, 550.
- Macerollo, A., et al., 2019. Peripheral trauma and risk of dystonia: what are the evidences and potential co-risk factors from a population insurance database? *PLoS One* 14, e0216772.
- Martino, D., et al., 2013. Extragenetic factors and clinical penetrance of DYT1 dystonia: an exploratory study. *J. Neurol.* 260, 1081–1086.
- Mathis, A., et al., 2018. DeepLabCut: markerless pose estimation of user-defined body parts with deep learning. *Nat. Neurosci.* 21, 1281–1289.
- Mink, J.W., et al., 1981. Ratio of central nervous system to body metabolism in vertebrates: its constancy and functional basis. *Am. J. Phys.* 241, R203–R212.

- Mitchell, R.W., et al., 2011. Fatty acid transport protein expression in human brain and potential role in fatty acid transport across human brain microvessel endothelial cells. *J. Neurochem.* 117, 735–746.
- Morris, A.A., 2005. Cerebral ketone body metabolism. *J. Inherit. Metab. Dis.* 28, 109–121.
- Moruno-Manchon, J.F., et al., 2017. Inhibiting sphingosine kinase 2 mitigates mutant huntingtin-induced neurodegeneration in neuron models of Huntington disease. *Hum. Mol. Genet.* 26, 1305–1317.
- Muthuraman, M., et al., 2008. Differentiating phase shift and delay in narrow band coherent signals. *Clin. Neurophysiol.* 119, 1062–1070.
- Muthuraman, M., et al., 2018. Cerebello-cortical network fingerprints differ between essential, Parkinson's and mimicked tremors. *Brain* 141, 1770–1781.
- Naismith, T.V., et al., 2004. TorsinA in the nuclear envelope. *Proc. Natl. Acad. Sci. USA* 101, 7612–7617.
- Nehlig, A., 2004. Brain uptake and metabolism of ketone bodies in animal models. *Prostaglandins Leukot. Essent. Fat. Acids* 70, 265–275.
- Nery, F.C., et al., 2011. TorsinA participates in endoplasmic reticulum-associated degradation. *Nat. Commun.* 2, 393.
- Ozelius, L.J., et al., 1997. The early-onset torsion dystonia gene (DYT1) encodes an ATP-binding protein. *Nat. Genet.* 17, 40–48.
- Paxinos, G., Watson, C., 2007. *The Rat Brain in Stereotaxic Coordinates*. Academic Press.
- Pyszkowski, J.A., Strosznajder, J.B., 2014. The key role of sphingosine kinases in the molecular mechanism of neuronal cell survival and death in an experimental model of Parkinson's disease. *Folia Neuropathol.* 52, 260–269.
- Rakhshandehroo, M., et al., 2009. Comparative analysis of gene regulation by the transcription factor PPARalpha between mouse and human. *PLoS One* 4, e6796.
- Rakhshandehroo, M., et al., 2010. Peroxisome proliferator-activated receptor alpha target genes. *PPAR Res.* 2010.
- Rauschenberger, L., et al., 2023. Peripheral nerve injury elicits microstructural and neurochemical changes in the striatum and substantia nigra of a DYT-TOR1A mouse model with dystonia-like movements. *Neurobiol. Dis.* 179, 106056.
- Ritche, M., et al., 2014. Functional connectivity relationships predict similarities in task activation and pattern information during associative memory encoding. *J. Cogn. Neurosci.* 26, 1085–1099.
- Romano, A., et al., 2017. Fats for thoughts: an update on brain fatty acid metabolism. *Int. J. Biochem. Cell Biol.* 84, 40–45.
- Schonfeld, P., Reiser, G., 2013. Why does brain metabolism not favor burning of fatty acids to provide energy? Reflections on disadvantages of the use of free fatty acids as fuel for brain. *J. Cereb. Blood Flow Metab.* 33, 1493–1499.
- Shashidharan, P., et al., 2000. Immunohistochemical localization and distribution of torsinA in normal human and rat brain. *Brain Res.* 853, 197–206.
- Sheehy, M.P., Marsden, C.D., 1980. Trauma and pain in spasmodic torticollis. *Lancet* 1, 777–778.
- Sivasubramanian, M., et al., 2015. Sphingosine kinase 2 and sphingosine-1-phosphate promotes mitochondrial function in dopaminergic neurons of mouse model of Parkinson's disease and in MPP+ -treated MN9D cells in vitro. *Neuroscience* 290, 636–648.
- Sokoloff, L., 1960. The metabolism of the central nervous system in vivo. In: Field, J., et al. (Eds.), *Handbook of Physiology—Neurophysiology*. American Physiological Society, Washington, D.C., pp. 1843–1864.
- van Hall, G., et al., 2009. Blood lactate is an important energy source for the human brain. *J. Cereb. Blood Flow Metab.* 29, 1121–1129.
- van Raalte, D.H., et al., 2004. Peroxisome proliferator-activated receptor (PPAR)-alpha: a pharmacological target with a promising future. *Pharm. Res.* 21, 1531–1538.
- Wagner, G.P., et al., 2012. Measurement of mRNA abundance using RNA-seq data: RPKM measure is inconsistent among samples. *Theory Biosci.* 131, 281–285.
- Wanders, R.J., et al., 2003. Peroxisomal fatty acid alpha- and beta-oxidation in health and disease: new insights. *Adv. Exp. Med. Biol.* 544, 293–302.
- Yang, C., et al., 2020. Rewiring neuronal Glycerolipid metabolism determines the extent of axon regeneration. *Neuron* 105 (276–292), e5.
- Yoon, M., 2009. The role of PPARalpha in lipid metabolism and obesity: focusing on the effects of estrogen on PPARalpha actions. *Pharmacol. Res.* 60, 151–159.